

# Modeling the functional network of primary intercellular $\text{Ca}^{2+}$ wave propagation in astrocytes and its application to study drug effects

Marcelo Pires<sup>a,b</sup>, Frank Raischel<sup>a,c</sup>, Sandra H. Vaz<sup>d,e</sup>, Andreia Cruz-Silva<sup>d,e</sup>, Ana M. Sebastião<sup>d,e</sup>, Pedro G. Lind<sup>a,f</sup>

<sup>a</sup>*Centro de Física Teórica e Computacional, Faculdade de Ciências, Universidade de Lisboa, Campo Grande 1649-003 Lisboa, Portugal*

<sup>b</sup>*Departamento de Física, Universidade Federal do Amapá, Jardim Marco Zero, 68903-419 Macapá/AP, Brazil*

<sup>c</sup>*Centro de Geofísica, Instituto Dom Luiz, Universidade de Lisboa, 1749-016 Lisboa, Portugal*

<sup>d</sup>*Instituto de Farmacologia e Neurociências, Faculdade de Medicina, Universidade de Lisboa, 1649-028 Lisboa, Portugal*

<sup>e</sup>*Unidade de Neurociências, Instituto de Medicina Molecular, Universidade de Lisboa, 1649-028 Lisboa, Portugal*

<sup>f</sup>*Institute für Physik and ForWind, Carl-von-Ossietzky Universität Oldenburg, DE-26111 Oldenburg, Germany*

## Abstract

We introduce a simple procedure of multivariate signal analysis to uncover the functional connectivity among cells composing a living tissue and describe how to apply it for extracting insight on the effect of drugs in the tissue. The procedure is based on the covariance matrix of time resolved activity signals. By determining the time-lag that maximizes covariance, one derives the weight of the corresponding connection between cells. Introducing simple constraints, it is possible to conclude whether pairs of cells are functionally connected and in which direction. After testing the method against synthetic data we apply it to study intercellular propagation of  $\text{Ca}^{2+}$  waves in astrocytes following an external stimulus, with the aim of uncovering the functional cellular connectivity network. Our method proves to be particularly suited for this type of networking signal propagation where signals are pulse-like and have short time-delays, and is shown to be superior to standard methods, namely a multivariate Granger algorithm. Finally, based the statistical analysis of the connection weight distribution, we propose simple measures for assessing the impact of drugs on the functional connectivity between cells.

**Keywords:** Signal Propagation, Cellular tissues, Complex Networks, Drug Tests

**PACS:** [2010] 87.18.Nq, 87.85.dm, 87.19.rp

## 1. Introduction

Astrocytes, which were long thought to perform only auxiliary functions in the brain, are known to exhibit complex patterns of  $\text{Ca}^{2+}$  waves propagating in their cellular network[1]. The basic biological mechanisms that underlies the functional links between astrocytes, leading to consecutive elevations in calcium signal[2, 3]. The predominant mechanism is mediated by ATP, which activates metabotropic P2Y receptors in the astrocytic membrane, leading to the formation of inositol-3-phosphate ( $\text{IP}_3$ ), which then signals to release calcium from the intracellular stores. Calcium elevation in an astrocyte leads to further release of ATP to the extracellular media, which quickly acts in receptors in the membrane of neighboring cells, leading to calcium elevations in those cells, which leads to a continuous cascade of  $\text{Ca}^{2+}$  signal propagation. Transfer of  $\text{IP}_3$  across gap-junctions (connexins) may also contribute for the calcium elevation[4], though in a minor degree[2, 5, 6]. Other recent studies have shown that intracellular  $\text{Ca}^{2+}$  oscillations are basically a form of correlated noise[7], which raises the question of stochasticity and reproducibility of the signal propagation and the corresponding network. While questions concerning the details of the propagating mechanisms remain an important mat-

ter of discussion[8], we are here interested in extracting insight from the inter-connectivity between cells by keeping track of  $\text{Ca}^{2+}$  signals.

Uncovering the functional connectivity of astrocytes in these networks provides a better understanding of the functionality of the astrocytic network itself, but also allows us to assess drug effects, not only at the single cell level, but also upon the spreading of the signal throughout the cellular tissue[8]. Such activity can be well characterized by measuring the concentration of calcium ions ( $\text{Ca}^{2+}$ ) using noninvasive techniques of calcium imaging. One of the most popular of such techniques uses fluorescent dye indicators, which bind selectively to free  $\text{Ca}^{2+}$  ions, undergoing a conformational change and consequently a variation in its fluorescence excitation and/or emission properties when bounded to  $\text{Ca}^{2+}$ . These variations can be used to evaluate changes in intracellular  $\text{Ca}^{2+}$  concentration. Here concentration is measured by the ratio  $R$  between maximum amplitudes at 340 and 380 nm, as illustrated in Fig. 1.

The evolution of  $\text{Ca}^{2+}$  concentration in each cell depends typically on the diffusion of the signaling molecules through the intercellular environment and on the direct connection from one astrocyte to its neighbors. While the former mechanism

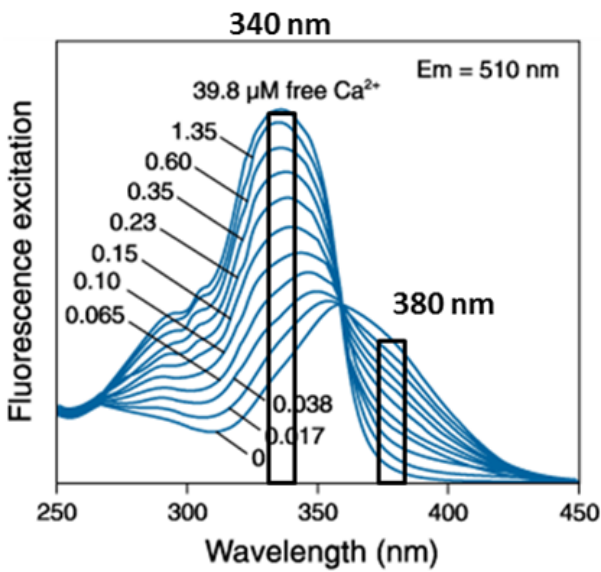
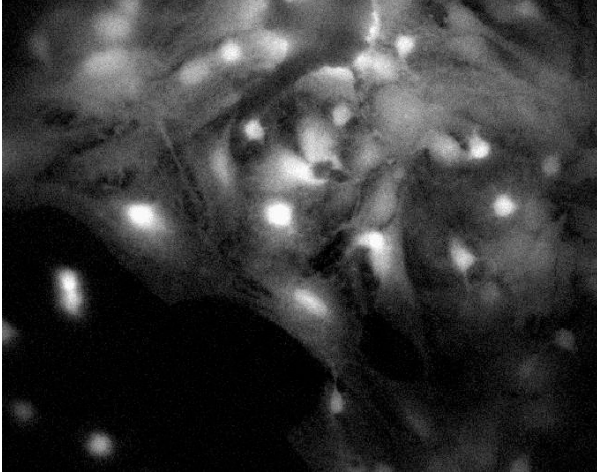


Figure 1: Set of 20 astrocytes observed through calcium imaging procedures. Bright regions indicate the location of cytoplasm and organelles, where the concentration of  $\text{Ca}^{2+}$  is higher than in the dark regions indicating the intercellular medium, where diffusion processes take place. Concentration is measured by the ratio  $R$  between the radiation emitted at 510 nm when cells are excited at 340 nm over emission upon excitation at 380 nm.

is slow, the latter is fast and dominates for measurement series with high sample rates. This study focuses on the latter case. Therefore, the series of measurements of  $\text{Ca}^{2+}$  concentrations at each cellular location reflects the flow of  $\text{Ca}^{2+}$ , and consequently the propagation of this ion from each cell to the neighboring ones. It should be noted that the brightening front generated at each cell does not necessarily propagate radially to its neighbors, since the physical connections between neighboring cells are heterogeneously distributed, which introduces spatial inhomogeneities in the signal propagation[4, 9].

One possible way to model  $\text{Ca}^{2+}$  signal propagation is through a bottom-up approach, where the kinetic constants of intracellular and intercellular signal pathways, the spatial distributions of connections and receptors in the tissue, and the relative importance of signal propagation mechanisms needs to be known and incorporated in a detailed mechanical simulation.

However, this approach is quite cumbersome and case dependent.

We argue, however, that the detailed physical structure of interconnected cells is not necessary to characterize the response of the interconnected tissue to a signal. For that one only needs to uncover the so-called functional connectivity between cells, which describes the synchronization patterns between the cells. While functional connectivity is at most loosely related to causal connectivity, it reflects the way the tissue as an interconnected structure of cells, responds to external stimuli, and how this functional network is changed when applying drugs.

Therefore, for our purposes, we focus here on the functional connectivity. Similar approaches to assess the functional connectivity in biological systems have already been presented, e.g. in islets of Langerhans from mouse pancreas tissue slices[10].

From the mathematical perspective, we quantify the connectivity and causality of information flow between the cells as a weighted graph. A graph is a collection of nodes interconnecting through edges according to some specific rules [11].

Our aim here is mapping the complex interactions and temporal information flow patterns to a much simpler representation. The graph is completely characterized by a single matrix, the adjacency matrix, whose entries are the weights of the edges between nodes. In case of cellular tissues, nodes represent the cells, and edges between them the functional connections between a respective pair of cells.

To reconstruct this graph we consider the paths connecting neighboring astrocytes in a confluent culture of astrocytes, used as a tissue model, analyzing the time series of  $\text{Ca}^{2+}$  concentration measurements observed at each astrocyte separately (see Fig. 2). From these experimentally measured synchronization patterns, we employ the correlation measures between the  $\text{Ca}^{2+}$  time series.

Standard algorithms exist for this problem, based in Granger causality[12, 13, 14]. However, although they can be adapted to suit multivariate non-stationary data series[15, 16], these methodologies assume the existence of a random process with a certain level of stationarity and then apply spectral analysis, decomposing the data series into a certain number of uncorrelated components, each one corresponding to a given spectral frequency.

For our particular case where one has sets of externally stimulated signals that are typically pulse-like and with short time-delays between them, a different approach must be considered, as will become apparent below.

Here, we show that these particular signals observed in signal propagation of astrocytic tissues can best be recovered by our simple and accurate procedure, which can also be applied for assessing the efficiency and irreversibility of drug infusion on the structure of the tissue, by studying signal propagation.

This report is organized as follows. We start in Section 2 by describing the general properties of the signal and then give a detailed account of our procedure. In particular, we argue that using the normalized covariance between astrocytes for specific time-lags enables one to quantify the connectivity of each pair of astrocytes. We then show that, for synthetic networks, our

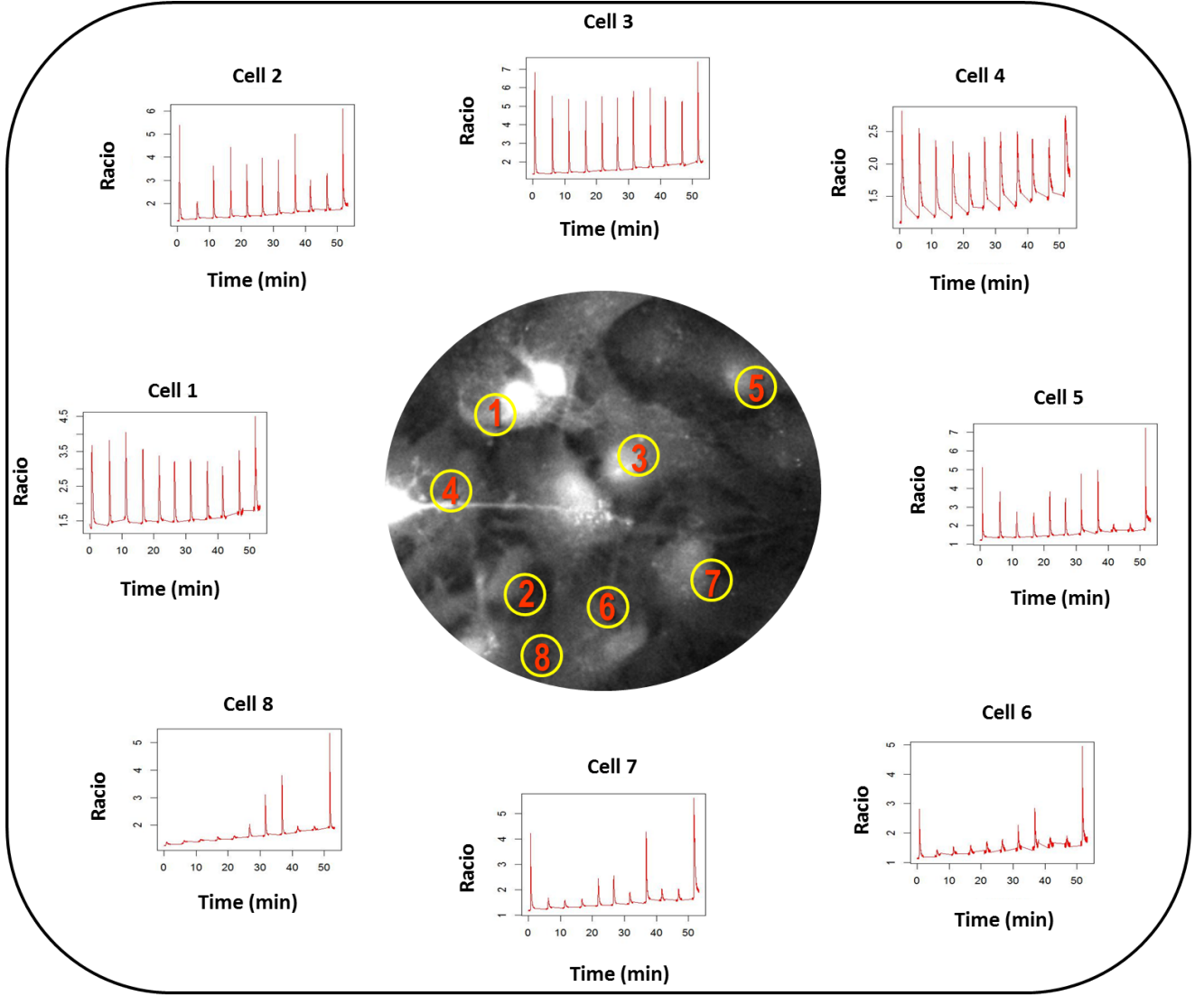


Figure 2: Intercellular  $\text{Ca}^{2+}$  signaling cascade. When one has a set of time series of the radiation ratio  $R$  measured at each cell of a tissue sample, how can one infer the flow of  $\text{Ca}^{2+}$  through the tissue? The central plot shows a case of eight signals extracted from the indicated positions, one per cell, forming the culture of confluent astrocytes that is used as a tissue model. In the ten surrounding signal plots, each plot shows the respective response of an individual cell to ten different ATP stimuli (see text) applied to cell 1. The final, eleventh peak shows the maximum cellular response, recorded by applying a supramaximal ATP stimulus ( $100\mu\text{M}$ ) to cell 1, and was not used in the analysis below.

procedure is more efficient and accurate than standard algorithms such as Granger causality. In Sec. 3 we describe the experimental setup and the data extracted from samples of living astrocyte tissues. In Sec. 4, we extract the connectivity networks for each sample and for each stimulus, using our procedure, and afterward analyze the moments of the weight distribution found for each tissue sample to discuss the effect of two drugs on the connectivity structure and the signal propagation, and the variability of the results. Finally, Sec. 5 concludes the paper giving also a brief description of how this method can be applied to drug tests. Our auxiliary model for creating synthetic signal data is described in Appendix A. The Granger method and algorithm is briefly described in Appendix B.

## 2. Extracting cellular functional connectivity

### 2.1. Properties of the experimental signal propagation

A brief description of the common numerical features of the  $\text{Ca}^{2+}$  cascade follows. A detailed description of the experimental setup can be found in Sec. 3.

In all experiments, cell 1 is externally stimulated 10 times, with  $10\mu\text{M}$  ATP (focally applied for 200 ms), the 11th peak being induced by a supramaximal concentration of ATP ( $100\mu\text{M}$ ) to test the maximal activity of the cell. The  $\text{Ca}^{2+}$  signal cascade is observed by measuring the intracellular  $\text{Ca}^{2+}$  levels, cf. Figs. 1,2, through the radiation amplitude ratio  $R$ .

The measured temporal signals, cf. Fig. 2, are a series of pulses, accompanied by an increasing trend, the latter not being of interest here. The signals are of similar shape, which is initially Gaussian, before decaying with a slower-than exponential

tail. The amplitudes, however, are widely varying. Generally speaking, it can be observed in this example that the stimulated cell 1—and also cell 4—have more or less constant signal amplitude ratios, whereas the cells farther away from cell 1 exhibit lower amplitudes and less regular peak heights. The signals are all delayed with respect to cell 1, although this crucial property is not visible at the resolution level provided by Fig. 1. This delay, specifically the delay in correlations related to it, is the cornerstone of our method of reconstructing the signal network.

## 2.2. Modeling functional connectivity strength from signal correlation

Following the experimental results, we propose a model to obtain the network of functional connectivity, i. e. the existence, direction and strength of network links between the network nodes, which are the cells, from the measured signal correlations. The result is then a network comparable to Fig. 3a.

We consider a number  $M$  of cells from which the  $\text{Ca}^{2+}$  can be measured composing the time series  $X_i(t)$ ,  $i = 1, \dots, M$  and  $t$  labeling time-steps. To derive the connectivity between a pair of cells, say  $i$  and  $j$ , we consider primarily how strong the corresponding signals,  $X_i(t)$  and  $X_j(t)$ , are correlated. Since we are dealing with signal propagation, one must also consider a time-delay  $\tau$  separating the two measures  $X_i(t)$  and  $X_j(t - \tau)$ . In particular, we assume that a proper choice of the value of  $\tau$  may completely reproduce at cell  $j$  the shape of the signal occurring previously in cell  $i$ , i.e.  $X_i(t) = X_j(t - \tau)$  for all times  $t = n\Delta t$ , modulo an attenuation factor. Here,  $\Delta t$  is the inverse of the sample rate taken for extracting the series of measurements composing the signal at steps  $n = 1, \dots, N$ , with  $N$  indicating the total number of measurements.

Typically, the signal at one cell is not completely reproduced in another cell, since the signal propagation involves various mechanisms, such as gap junction transport and diffusion. To determine how strong the signals are correlated, we take their covariance with a time-delay  $\tau$ :

$$C(X_i, X_j, \tau) = \frac{\sum_{t=\tau}^N (X_i(t) - \bar{X}_i)(X_j(t - \tau) - \bar{X}_j)}{(N - 1)\sigma_i\sigma_j} \quad (1)$$

where  $\bar{X}_i$  and  $\sigma_i$  stand for the average and standard deviation of signal  $X_i(t)$  respectively. This measure has the properties  $C(X_i, X_i, 0) = 1$  and  $\lim_{\tau \rightarrow \infty} C(X_i, X_j, \tau) = 0$ .

The value of the covariance between the signals at two neighboring cells may vary depending on the type of stimulus applied at the source-cell. Also, when repeatedly applying the same stimulus to the same array of cells, signal propagation may be altered by aging or learning effects. One would also expect that the effect of drugs is reflected by the covariance, such that, when the covariance increases in absolute value, it could indicate an excitatory effect of the stimulus substance. Or, when it decreases, it could reveal an inhibitory effect.

We stress once more that, while it remains only a hypothesis that the strength of the connection between two cells can be ascertained from the covariance their functional connectivity is indeed reflected in the covariance: the larger the covariance between two signals is in absolute value, the stronger the connec-

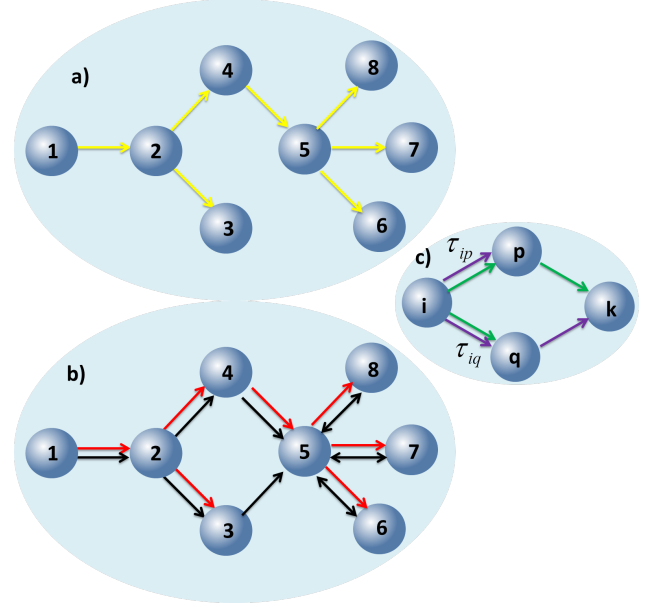


Figure 3: (a) A sample directed graph of functional connectivity as it can be extracted by our method, here for  $M = 8$  interconnected (artificial) astrocytes. Nodes represent the cells (blue bullets) and edges represent their connections (yellow arrows). (b) The connections can be evaluated from the time series at each node using two different procedures: Granger causality[12, 13, 14] (black arrows) or our method (red arrows). Comparing the results with the synthetic network of astrocytes in (a), our method can be taken as better for this particular purpose (see text and Fig. 7). (c) Particular cases of signal correlations, namely Pearson coefficient equal to one, may represent different but equivalent signal propagation topologies.

tion between the functional behavior of the corresponding cells should be.

Figure 4 shows the covariance between two astrocytes in the sample showed in Fig. 1. Depending on the value of the delay  $\tau$ , the covariance between two series can be large (close to 1 or  $-1$ ) or small (close to 0). The successive maxima shown in Fig. 4 correspond to distinct stimuli.

However, the covariance alone does not suffice for showing how strongly connected two astrocytes are. Indeed, the covariance for different delays correspond to different interaction modes, rates and paths joining two cells. Here, we focus in the “first” interaction mode, corresponding to the fastest path propagating the signal from the unique source-cell to each of the other cells in the tissue. We assume that detecting for instance a reversible or irreversible effect of a drug in the rapidity of these propagating paths is sufficient to determine the reversible or irreversible effect in the tissue.

To determine the fastest paths, the time-delay in Eq.(1) must also be considered, specifically the smallest one that maximizes the covariance: the delay needed for characterizing the connection between astrocytes is the lowest delay for which a local maximum of the covariance is observed. This value will be referred to as  $\tau_{max}$ , cf. Fig. 4, and the corresponding covariance is henceforth called  $C_{max} = C(X_i, X_j, \tau_{max})$ .

The time-delay  $\tau_{max}$  in fact measures the typical time for the signal to propagate from astrocyte  $i$  to astrocyte  $j$ . Notice that we do not consider the relative distances of the cells because, as



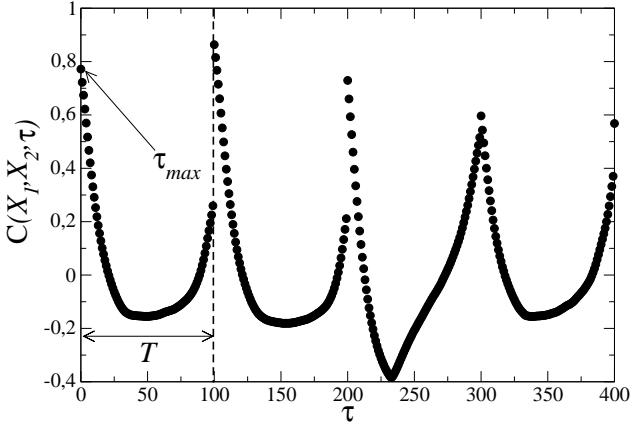


Figure 4: The covariance in Eq. (1) between the two cells 1 and 2, shown in Fig. 3, as a function of time-delay  $\tau$ . Here,  $T$  is the time-window between successive stimuli. Typically, during each  $T$  period, the covariance decreases from a maximum value to a minimum. The value of  $\tau_{max}$  giving the delay for which the covariance is maximized is the lowest time-lag corresponding to a relative maximum.

mentioned in the introduction above, the medium in which the signals propagates is highly heterogeneous and therefore preferential and non-preferential pathways of signal propagation exist and the geometrical distance is not a suitable criterion for signal propagation velocity[9].

In the particular situation that a cell propagates its signal to two neighbors with neither delay nor dumping, the respective covariances are exactly one, see Fig. 3c. In this case both situations drawn with blue and green arrows are equivalent and indistinguishable. Either one, and only one, of them is known to connect the set of cells.

If the delay  $\tau_{max}$  that maximizes the covariance between two astrocytes is small, it means that they should be closely connected and the corresponding connection should be strong. If the time-delay is large compared to other pairs, the corresponding strength should be small compared to those other pairs. Therefore, the weight of the connection is reasonably assumed to be proportional to the inverse of the delay  $\tau_{max}$ .

Combining all the considerations above we define the strength  $w_{ij}$  of the connection between astrocytes  $i$  and  $j$  as

$$w_{ij} = \frac{|C_{max}(X_i, X_j, \tau_{max})|}{\tau_{max} + 1}, \quad (2)$$

where one unit in the denominator is added for convenience, to avoid singular behavior. Notice that the weight  $w_{ij}$ , being the quotient between correlation of two signals and time, can be interpreted as a correlation flux, which in this case measures the causality – and not the strength – of the flow of information between cells.

Still, the weight value alone cannot reveal the structure of single signals through the tissue, as we explain next<sup>1</sup>.

<sup>1</sup>The full implemented algorithm can be shared for research purposes. For that, please contact the authors.

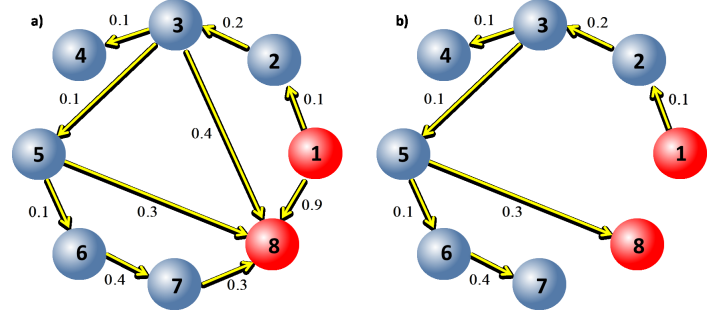


Figure 5: Illustration of the computation of optimum paths. (a) At each edge the corresponding delay  $\tau_{max}$  is indicated. In this example the optimum path between cells 1 and 8 is  $P(1, 8) = \{1, 2, 3, 5, 8\}$ , because this path combines the least time cost (0.7) and greatest number of edges (4). See Tab. 1. (b) Consequently, the connections  $\{1, 8\}$ ,  $\{3, 8\}$  and  $\{7, 8\}$  are redundant and therefore are filtered out by the procedure.

Path	Time Cost	Number of Edges
$\{1, 8\}$	0.9	1
$\{1, 2, 3, 8\}$	0.7	4
$\{1, 2, 3, 5, 8\}$	0.7	5
$\{1, 2, 3, 5, 6, 7, 8\}$	1.2	7

Table 1: Time cost and number of edges of all paths between cells 1 and 8 in the example sketched in 5.

### 2.3. Constraints for signal propagation

For any pair  $i$  and  $j$ , the strength  $w_{ij}$  is typically a non-zero value. Therefore, by solely considering the values of  $w_{ij}$  computed as in Eq. (2), one cannot immediately infer the structure shown in Fig. 3a, since typically there is a non-zero covariance for *any* pair of cells. A final step is still necessary to filter out redundant connections.

The filter is based on two simple constraints for the connections. First, there is one single source-cell characterized by having one or more outgoing connections but no incoming connection. In all experiments shown, this is the first cell,  $i = 1$ . Second, all cells, different from the source-cell, have only one incoming connection, but can have several outgoing connections. These two constraints are the sufficient and necessary ones for cell-to-cell signal propagation, which is the situation we are considering here.

From these two constraints the task reduces to extract the incoming functional connection of each cell that establishes an optimal (fastest) path from the source-cell to it. We say that a path  $P_O(i, j)$  between two cells,  $i$  and  $j$ , is the optimum path between these cells if it has the minimum (total) time-delay cost from all possible path  $P(i, j)$ . In case one has more than one path corresponding to the minimum time-delay, one should choose the path maximizing the number of connections, in order to minimize the time between each two adjacent cells in the path. Figure 5, together with Tab. 1, illustrates how the optimum path between each pair of cells is computed.

Starting from the source-cell, we traverse the network using a burning breadth-first algorithm[17]: start at a root node and inspect all its neighbors; for each of those neighbors, inspect

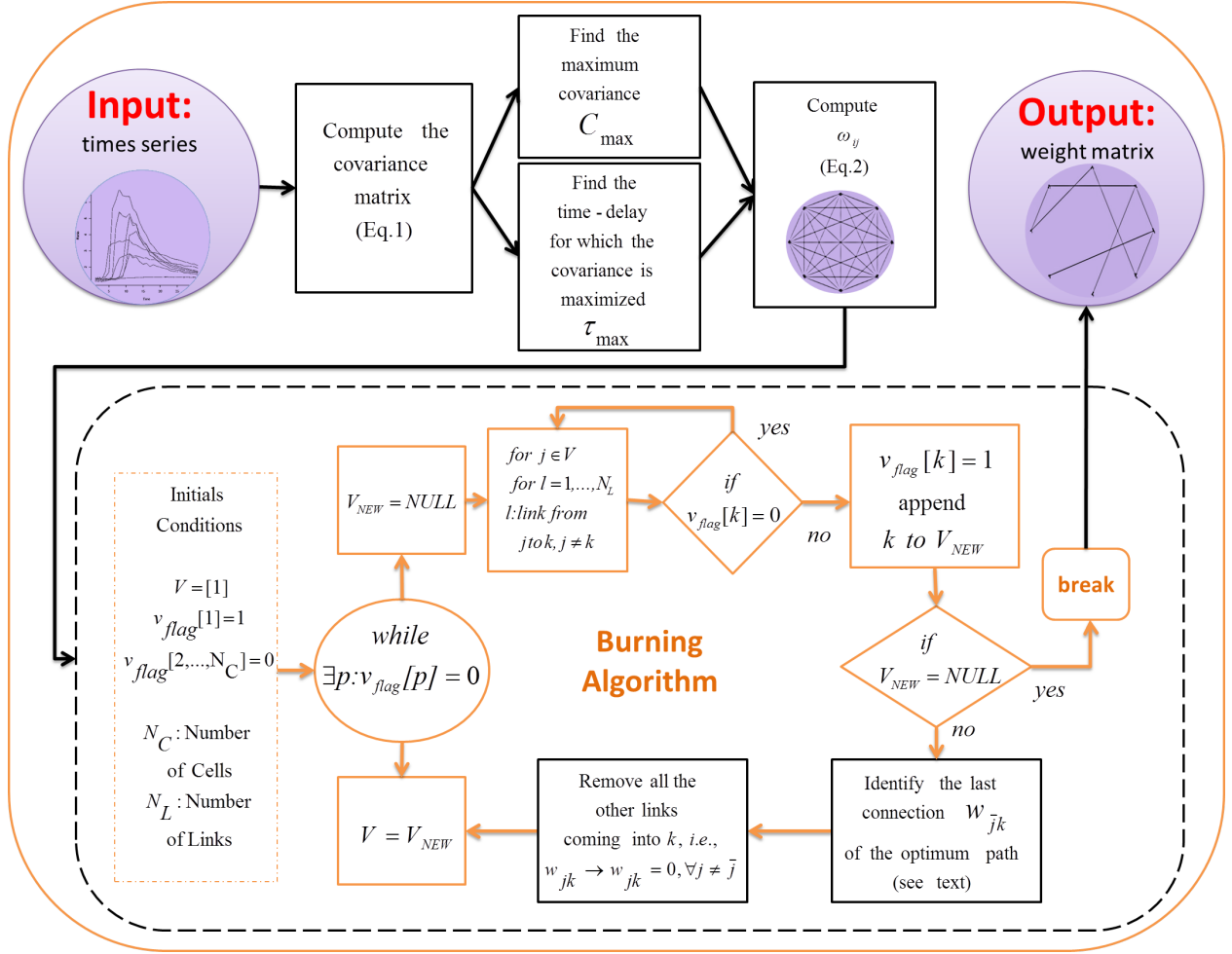


Figure 6: Infography of the algorithm for extracting the connectivity network of astrocytic tissues (see Sec.2).

their neighbor nodes which were still not visited; and so on. Then, for the source-cell we compute the optimum path from it to each one of its neighbors, removing all redundant incoming connections of each neighboring cell. We iteratively repeat this procedure for each one of these neighbors, and therefore for all cells. Figure 6 summarizes the full algorithm.

#### 2.4. Verification of the network reconstruction algorithm with a simple model of $\text{Ca}^{2+}$ signal propagation

In order to numerically verify the reliability of our reconstruction algorithm, described in the previous sections 2.2 and 2.3, we will consider in this section a synthetic network of cells, as sketched in Fig. 3a, joined by directed connections (yellow arrows). We simulate the information flow through these artificial networks by a simple auxiliary model of information flow described in detail in Appendix A. At cell 1 a Gaussian stimulus  $X_1(t)$  is introduced. Here,  $X_1$  corresponds to the experimental ratio  $R$  of both radiation amplitudes (see Fig. 1) measured at cell 1.

By prescribing a time-delay to each connection, which controls the necessary delay for the signal to propagate to the neighboring cells, we extract the series of values composing the signal at each of the other cells. Using the algorithm described in

the previous subsections, we were able to accurately uncover the connectivity structure sketched in Fig. 3a with yellow arrows solely by analyzing the separated signals. In Fig. 3b we indicate the result of our reconstruction with red arrows and compare it with results obtained from the standard Granger algorithm for multivariate data[13] (black arrows). Comparison with Fig. 3a shows the accuracy of our reconstruction, whereas the Granger model identifies spurious connections not present in the network. Next we carefully compared our algorithm with the standard Granger causality, analyzing a set of 100 artificial networks of 11 synthetic cells (10 connections). For details on the generation of synthetic data we again refer the reader to Appendix A, and for details on Granger causality procedures see Appendix B.

Figure 7 shows the frequency of artificial networks that correctly detect a given percentage of connections (efficiency). As can be clearly seen, in all cases at least 50% of the connections were properly extracted, and typically the percentage of connections correctly identified lies between 80% and 90%. In comparison with the standard Granger algorithm (red histogram), one concludes that for these signal-propagating networks the above procedure shows a high efficiency.

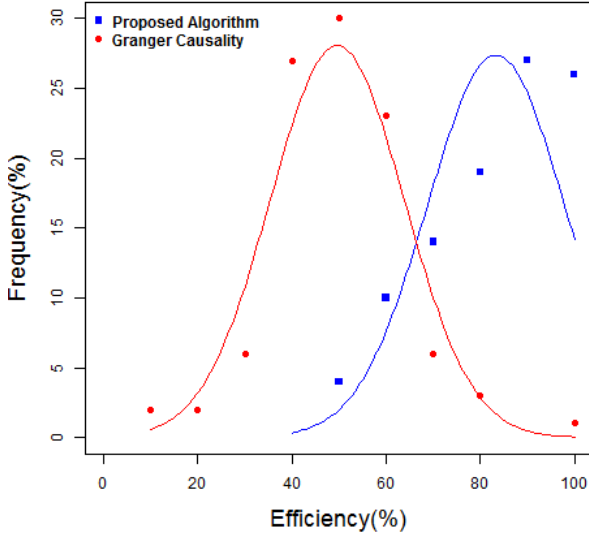


Figure 7: Testing the algorithm for extracting the connectivity network in living tissues of astrocytes. For the procedure described in Sec. 2 (blue histogram) all networks show a correctness larger than 50% and most of them reach 80–90%. Such correctness is significantly larger than the one obtained with standard Granger causality (red histogram). The plot shows the percentage of connections correctly extracted from 100 artificial networks, each with 11 cells and 10 connections.

Here efficiency  $e$  was computed directly from the number  $N_c$  of connections that were correctly predicted and the number of connections  $N_e$  equivalent to the original networks, as sketched in Fig. 3c, yielding  $e = (N_c + N_e)/N_T$ , being  $N_T$  the total number of connections correctly predicted. For our algorithm the total number of connections equals the number of cells minus one,  $N_T = n_c - 1$ . For the Granger algorithm  $N_T$  is variable and lies between  $n_e - 1$  and  $n_e(n_e - 1)$ , since it is insensitive to the constraints for cell-to-cell propagation introduced above.

It should be noted that there are two fundamental differences between Granger’s method and ours. First, our procedure considers a connectivity matrix weighted by the time-lag between signals. Second, it introduces two constraints necessary for uncovering the so-called primary graph in the particular case of externally stimulated tissues of interconnected cells. From these tissues one extracts multivariate signals that result from one single source signal – the external stimulus – which propagates throughout a spatially extended system. By uncovering the primary graph, our procedure will not guarantee that reversal connections do not exist. Still, focusing on the primary graph, we see that it retrieves first order effects of the stimulus in the interconnected functional structure among cells propagating the signal, particularly in the case when a drug is used. We show below that these effects are complementary to the usual effects uncovered through standard drug tests (see Fig. 8 below). With our procedure, non-distinguishable connections are mutually exclusive, avoiding redundant connections.

### 3. Experimental setup and data extraction

As mentioned above in Sec. 1, activation of specific membrane receptors localized in the astrocytic plasma membrane triggers a rapid and brief rise of intracellular  $\text{Ca}^{2+}$  concentration in this cell, which promotes the release of gliotransmitters that will lead to the increase of intracellular  $\text{Ca}^{2+}$  concentration on a neighboring astrocyte. Thus, stimulation of a single astrocyte in culture, with ATP (adenosine-5’-triphosphate), induces intracellular  $\text{Ca}^{2+}$  elevation in the stimulated cell, which is then followed by  $\text{Ca}^{2+}$  increases in neighboring astrocytes.

The transmission of intercellular  $\text{Ca}^{2+}$  signals between astrocytes is achieved through two distinct pathways: (i) release of gliotransmitters that will bind receptors located on neighboring astrocytes, and/or (ii)  $\text{Ca}^{2+}$  itself, or a  $\text{Ca}^{2+}$  liberating second messenger (as  $\text{IP}_3$ ) permeate gap junction channels and then act on similar intracellular targets in neighboring coupled cells.

The calcium signal, as the ones recorded in the top plots of Fig. 8, corresponds to a calcium signal by one cell, i.e. the variation of the fluorescence ratio, proportional to calcium concentration within the cell versus time. In a monolayer culture of astrocytes, such as the ones studied here, the calcium signal propagates from one astrocyte to another creating a propagating calcium wave. The propagation velocity of  $\text{Ca}^{2+}$  waves reaches  $28.2 \mu\text{m/s}$ [1] and it is also known that intracellular velocity ranges from  $9.4$  to  $61.2 \mu\text{m/s}$ [18]. Thus, in order to have intracellular  $\text{Ca}^{2+}$  waves[19] that could be used to uncover the connections between the astrocytes we performed calcium imaging using primary cultures of cortical astrocytes. For the results shown in Fig. 8 we have a statistical significance of  $P < 0.05$  (Students t-test) for the hypothesis that the (Gaussian) distribution is the same when the signal amplitude during drug perfusion, upon ATP stimulation, is compared with the responses immediately before drug perfusion (control).

Primary cultures of cortical astrocytes from Wistar rats (0-2 days old) were prepared as reported previously[20] and in accordance with Portuguese laws and the European Union Directive 86/609/EEC on the protection of Animals used for Experimental and other scientific purposes.

For calcium measurements, microglia contamination was minimized by following a standard shaking procedure[21]. After six days in culture (DIC 6), cells in the T-75 culture flasks were shaken for 4-5h at  $37^\circ\text{C}$ , the supernatant was removed and DMEM supplemented medium was added. At DIC 7, the T-75 culture flasks were shaken again for 2-3 hours at  $37^\circ\text{C}$ , the supernatant containing mostly microglia was removed and then cells were washed once with PBS. After removing microglia contamination, astrocytes to be used in calcium imaging experiments were plated ( $7 \times 10^4$  cells/ml) in  $\gamma$ -irradiated glass bottom microwell dishes. Before plating, cells were gently detached by trypsinization (1% trypsin-EDTA) for 2 minutes, the process being stopped by the addition of 4.5 g/l glucose DMEM medium containing 10% fetal bovine serum with 0.01% antibiotic/antimycotic.

Astrocytes were loaded with the  $\text{Ca}^{2+}$ -sensitive fluorescent dye fura-2 acetoxymethyl ester (fura-2 AM; 5M) at  $22^\circ\text{C}$  for 45 minutes. After loading, the cells were washed three times

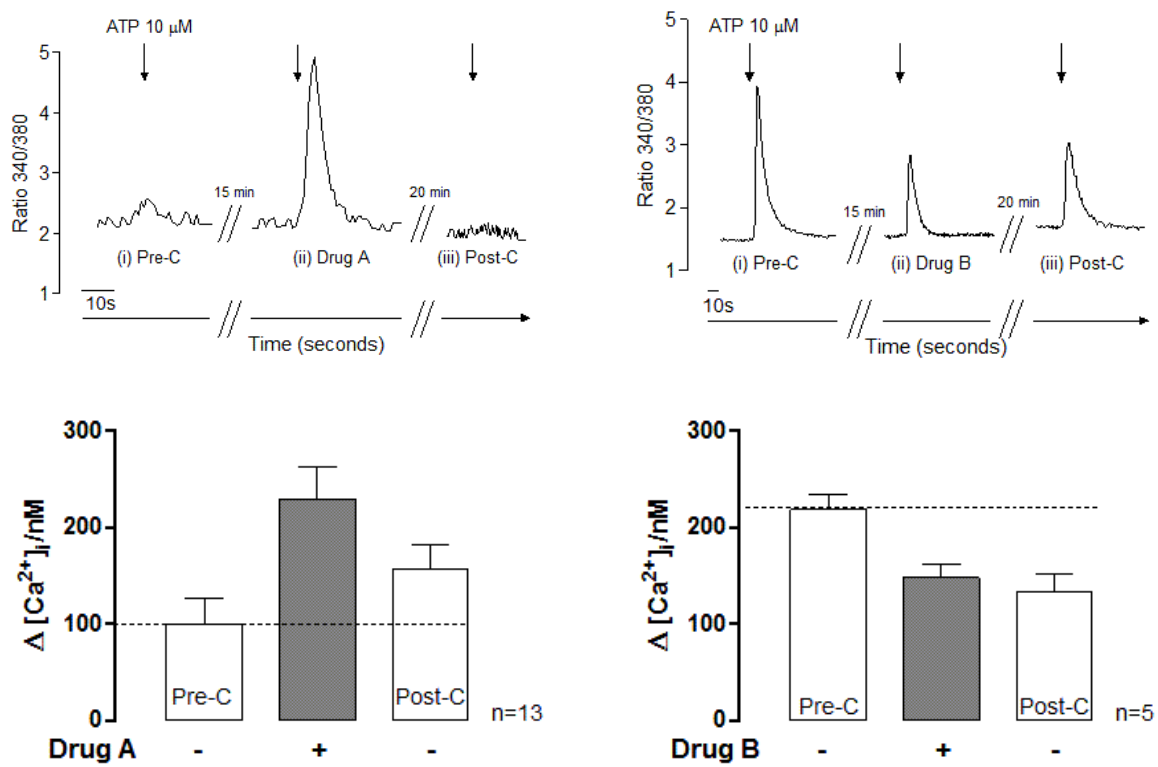


Figure 8: For determining if a drug is inhibitory or excitatory or to determine if its effects are reversible or not, one needs to observe the  $R$  ratio for three different moments: (i) before applying the drug (Pre-C), (ii) during the effect of the drug and after (iii) washing out the drug (Post-C). In the plots above we plot the  $R$  amplitude for these three instants using two different drugs drug A (left) and drug B (right). While drug A shows an excitatory and reversible effect, drug B is inhibitory and irreversible. In the plots below the averages of  $\text{Ca}^{2+}$  concentration for a total of ten experiments are shown. Statistical significance of the drug effect is  $P < 0.05$ . Drug A: 4-[2-[[6-Amino-9-(N-ethyl- $\beta$ -D-ribofuranuronamidosyl)-9H-purin-2-yl]amino]ethyl]benzene]propanoic acid hydrochloride; Drug B: N6-Cyclopentyl-9- $\beta$ -D-Ribofuranosyl-9H-purin-6-amine. Throughout the experiments, ATP (10  $\mu\text{M}$ ) was used as the stimulus to evoke  $\text{Ca}^{2+}$  signals. ATP was pressure applied for 200 ms (arrows in (a) and (b)) through a micropipette placed over the cells.

in external physiological solution (composition in mM: NaCl 125, KCl 3,  $\text{NaH}_2\text{PO}_4$  1.25,  $\text{CaCl}_2$  2,  $\text{MgSO}_4$  2, D(+)-glucose 10 and HEPES 10; pH 7.4 adjusted with NaOH)[22].

Dishes were mounted on an inverted microscope with epifluorescent optics (Axiovert 135TV, Zeiss) equipped with a xenon lamp and band-pass filters of 340 and 380 nm wavelengths. Throughout the experiments, the cells were continuously superfused at 1.5 ml/min with physiological solution with the aid of a peristaltic pump. Calcium signals were induced by ATP, applied focally, for 200 ms, through a FemtoJet microinjector (Eppendorf, Hamburg, Germany), coupled to an ATP (10  $\mu\text{M}$ ) filled micropipette placed under visual guidance over a single astroglial cell.

In this study we address the two following drugs: 4-[2-[[6-Amino-9-(N-ethyl- $\beta$ -D-ribofuranuronamidosyl)-9H-purin-2-yl]amino]ethyl]benzene]propanoic acid hydrochloride, henceforth named as “Drug A”, and N6-Cyclopentyl-9- $\beta$ -D-Ribofuranosyl-9H-purin-6-amine, henceforth named as “Drug B”. Both drugs were added to the external solution under perfusion. Changeover of solutions was performed by

changing the inlet tube of the peristaltic pump from one flask to another; changeover of solutions with equal composition did not lead to appreciable changes of the responses. In each experiment and for each cell, responses to the stimulus (pressure applied ATP) were first obtained in the absence of the drug (control, Pre-C), then in the presence of the drug, after changeover of solutions, and lastly after returning to the drug free conditions (washout, Post-C). Image pairs obtained every 250 ms by exciting the preparations at 340 and 380 nm were taken to obtain ratio images. Excitation wavelengths were changed through a high speed wavelength switcher, Lambda DG-4 (Sutter Instrument, Novato, CA, USA), and the emission wavelength was set to 510 nm. Image data were recorded with a cooled CCD camera (Photometrics CoolSNAP fx) and processed and analyzed using the software MetaFluor (Universal Imaging, West Chester, PA, USA).

Regions of interest were defined manually over the cell profile. Typically one chooses the cytoplasmic region for measuring the ratio  $R$ , given preference to the brightest regions in each astrocyte appearing in the photo images during one stimulus.



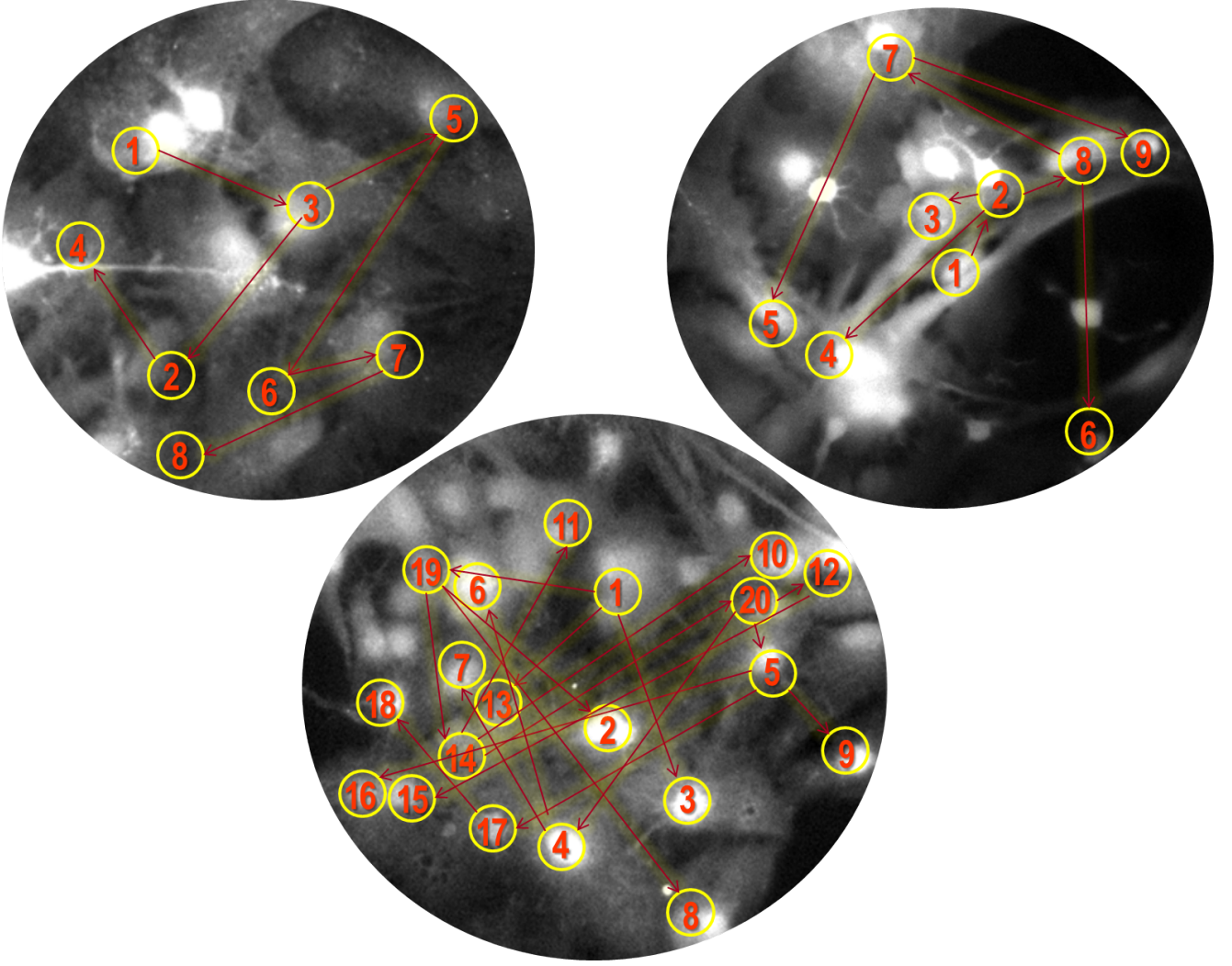


Figure 9: Three different astrocytic cultures with the corresponding derived network structure of  $\text{Ca}^{2+}$  signal propagation. Circles denote the location of spots where the signal was measured, namely in the cytoplasm. From the connectivity between cells and its evolution through a succession of ATP stimuli, one is able to evaluate relevant effects of the perfused drug on the culture (see text).

It is important to know whether the effect of a certain drug is inhibitory or excitatory, as well as whether it is reversible or irreversible. To that end we compute the ratio  $R$  (induced by ATP application) at three different time steps: before introducing the drug (left), in the presence of the drug (middle), and after washing out the effect of the drug (right). At each one of these moments one measures the magnitude of  $R$ , having values respectively  $R_{H_1}$ ,  $R_D$  and  $R_{H_2}$ . If  $R_D < R_{H_1}$  the drug has an inhibitory effect, while in the opposite case,  $R_D > R_{H_1}$  the drug proves to be excitatory. In our case one sees that the effect of drug A is excitatory (Fig. 8, top left) while the effect of drug B is inhibitory (Fig. 8, top right).

To ascertain the reversibility of drug effects one takes in addition the magnitude  $R_{H_2}$ . If  $R_D - R_{H_1} \sim R_D - R_{H_2}$  the effects are reversible. If not they should not be reversible, yielding typically  $R_D \sim R_{H_2}$ . In the case illustrated in Fig. 8, drug A is reversible while drug B is irreversible.

Notice that, the responses in left plot of Fig. 8 are from one cell. Responses from the right plot are from another cell and

another culture. The stimulation parameters in the condition illustrated in the top-left plot of Fig. 8 were empirically adjusted (by changing the relative position of the stimulating electrode) to induce a weak response under control conditions since the protocol was designed to test the influence of a drug known to have excitatory actions. Drug A is a well known and selective agonist of excitatory adenosine A2A receptors, known to be present in astrocytes[20]. The stimulation parameters in the condition illustrated in top-right plot of Fig. 8 were empirically adjusted (by changing the relative position of the stimulating electrode) to induce a stronger response under control conditions since the protocol was designed to test the influence of a drug known to have inhibitory actions. Drug B is a well known and selective agonist of inhibitory adenosine A1 receptors, also known to be present in astrocytes[23]. Importantly, within each panel, the responses shown are all from the same cell, under exactly the same stimulation conditions. Once set they were not changed up to the end of the recording period. The difference being absence or presence of the drug in the perfusion solution.

As we will see in the next section, by assessing the connectivity network for each set of cells in one culture of astrocytes we will be able to provide additional insight to the effect of one drug in the living tissue.

#### 4. Assessing drug effects from cellular connectivity

The standard procedure described in Sec. 3 for evaluating the excitatory and inhibitory effects of one drug or their reversible or irreversible character will in this section be extended to a broader context. Indeed, the approach done in the previous section considered the signal's total amplitude observed in the entire tissue sample. Now, using the method introduced in Sec. 2 allows us to retrieve the full structure of the connectivity network through which the injected stimulus propagates. In Fig. 9 three tissue samples are shown with their respective connectivity network for one particular stimulus. Next, we apply this procedure to a succession of ten stimuli in each tissue sample shown in Fig. 9. For each stimulus, the connectivity network is defined by the weight matrix  $w_{ij}$ , quantifying the signal propagation between all sender cells  $i$  and all receptor cells  $j$ .

For instance, while a drug may have an inhibitory effect on the amplitude, reducing the overall signal strength, it may simultaneously change the signal propagation network in a way that the signal, though weaker, propagates more easily, i.e. it has a facilitatory effect in the propagating structure. We introduce four additional quantities, each one of them reflecting the facilitatory or inhibitory – and reversible or irreversible – effects induced by a particular drug. As does  $w_{ij}$ , these additional properties characterize not the intensity of the signal but the stronger or weaker ability of the signal to propagate throughout the tissue, i.e. the causality of the information flow. Therefore, they can be taken as properties complementary to the amplitude.

The four additional quantities are all computed directly from the weight  $w_{ij}$  introduced above, using the auxiliary quantity  $\bar{w}_{ij} = (1/10) \sum_{T=1}^{10} w_{ij}(T)$  ( $T = 1, \dots, 10$ ), the average of the weight between each pair of cells, over the ten experimental phases. By ascertaining how the weights  $w_{ij}$  change from one stimulus to the next, we are able to determine the effects of the substance in the tissue, which is reflected by the moments of the weight distribution.

The first moment of the distribution is simply

$$\langle w \rangle(T) = \frac{1}{L} \sum_{i \neq j} w_{ij}(T), \quad (3)$$

with  $L$  indicating the total number of connections. While the set of values  $\bar{w}_{ij}$  represents the time-average strength of one single connection in time,  $\langle w \rangle(T)$  indicates the average weight – or flux – per connection in the tissue for a particular stimulus at time  $T$ .

The second moment is important for ascertaining how influential is a particular drug in inducing a variation of the weight between two connected cells. It is computed by accounting for the fluctuations around the means  $\bar{w}_{ij}$  and averaging them over

the  $L$  connections:

$$\sigma^2(T) = \frac{1}{L-1} \sum_{i \neq j} (w_{ij}(T) - \bar{w}_{ij})^2. \quad (4)$$

When  $\sigma = 0$  it implies that the connectivity network is precisely the same for all stimuli and therefore the drug has no influence in the weights. The larger the value of  $\sigma$  is, the stronger the influence of the drug to induce a variation in each connection. Typically, large fluctuations are more probable when the average weight is also large. Therefore, to remove this scaling effect, we consider the normalized second moment,  $\sigma/\langle w \rangle$ , which quantifies the fluctuations with respect to the observed average weight. We call this coefficient the sensitivity coefficient.

For evaluating how powerful a drug is in weakening or strengthening the connectivity between each pair of cells we consider the third moment of the weight distribution:

$$\mu^3(T) = \frac{1}{L} \sum_{i \neq j} (w_{ij}(T) - \bar{w}_{ij})^3. \quad (5)$$

When  $\mu = 0$  it means that the amount of connections with a strength below average is the same as the amount of connections with a strength above it. If  $\mu \neq 0$  the weight distribution is asymmetric. A positive value indicates that the values of the weights concentrate on the right-side of the distribution, i.e. there are few weak connections, while a negative value indicates that there are few strong connections. Consequently, when a stimulus leads to a connectivity network with a larger (smaller)  $\mu$  value than previously, it has a strengthening (weakening) effect on the connectivity of the tissue. Similarly to the second moment, we consider  $\mu/\sigma$ , normalized to the standard deviation  $\sigma$ . We call this coefficient the strengthening coefficient.

A fourth measure is added to these three moments, which we call variability  $\eta$ . It is a function of the stimulus  $T$  that evaluates how much the weights between each pair of cells varies from one stimulus to the next one:

$$\eta(T) = \frac{\sum_{i,j} |w_{i,j}(T+1) - w_{i,j}(T)|}{\sum_{i,j} |w_{i,j}(T+1) + w_{i,j}(T)|}. \quad (6)$$

The variability takes values between zero, when all connections remain the same from one stimulus to the next one, and one, when all connections switch from zero at  $T$  to one at  $T+1$  or vice-versa. The larger the variability the broader the overall induced change in the connectivity network.

For each tissue sample we considered a succession of typically ten stimuli, similarly to what was done above. The first two stimuli were applied in the absence of drugs (buffer) in order to uncover the tissue connectivity when not subjected to drugs. Then one of two drugs, herein referred to as drug A and drug B, were applied and the astrocytes stimulated four times. Drugs were then removed from the bath and the astrocytes stimulated again four times (washout period).

Figure 10 shows the four coefficients,  $\langle w \rangle$ ,  $\sigma/\langle w \rangle$ ,  $\mu/\sigma$  and  $\eta$ , measured for each stimulus. As for measuring the R ratio in Fig.8, we define a drug effect as inhibitory if  $R_D < R_{H_1}$ , or

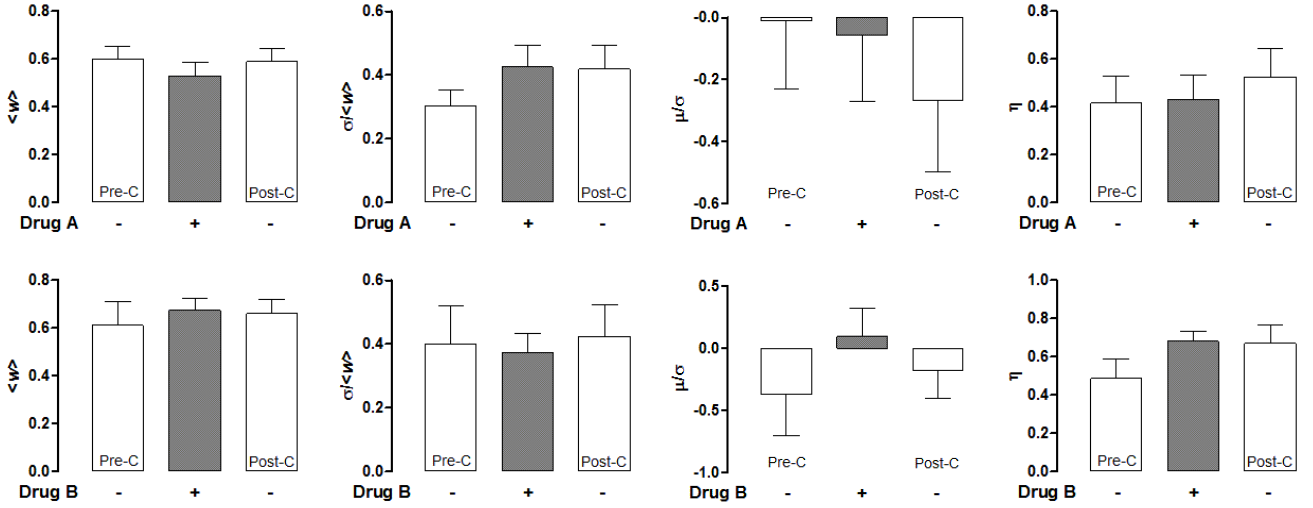


Figure 10: Assessing the robustness and activity of samples of astrocytic tissues throughout a series of ten stimuli: two initial stimuli (Pre-C), four drug A (first row) or drug B (second row) and four washout (Post-C). Drug A: 4-[2-[[6-Amino-9-(N-ethyl- $\beta$ -D-ribofuranuronamidosyl)-9H-purin-2-yl]amino]ethyl]benzene]propanoic acid hydrochloride; Drug B: N6-Cyclopentyl-9- $\beta$ -D-Ribofuranosyl-9H-purin -6-amine. From left to right one sees result for: flux  $\langle w \rangle$  (first column) in Eq. (3), sensitivity  $\sigma/\langle w \rangle$  (second column) in Eq. (4), strengthening  $\mu/\sigma$  (third column) in Eq. (5), variability  $\eta$  (fourth column) in Eq. (6). Here we use a total of ten experiments.

Property	Drug A	Drug B
Amplitude (Fig. 8)	+ (Rev.)	- (Irrev.)
Flux $\langle w \rangle$ (Fig. 10, 1st col)	0	0
Sensitivity $\sigma/\langle w \rangle$ (Fig. 10, 2nd col)	+ (Irrev.)	0
Strengthening $\mu/\sigma$ (Fig. 10, 3rd col)	0	0
Variability $\eta$ (Fig. 10, 4th col)	0	+ (Irrev.)
Correlation $\rho$ (Fig. 11)	+ (Irrev.)	+ (Rev.)

Table 2: Table of evaluation properties for the drugs, drug A and drug B, in signal amplitude and the properties assessing the structure of the signal propagation network. For each property we indicate whether its effects are facilitatory (+) or inhibitory (-) and reversible (Rev.) or irreversible (Irrev.). Zero indicates no statistical significance in a T-test among a total of ten experiments. Last row shows the correlation (see text), which deviates from the purely random case  $\rho = 1/4$ , except when applying drug B (see Fig. 11).

as exhibitory if  $R_D > R_{H_1}$ , and the classification as reversible or irreversible is based on the comparison of  $R_D - R_{H_1}$  and  $R_D - R_{H_2}$ . In Tab. 2 we present a summary of the main results from Fig. 10, where “0” indicates no statistical significance in a T-test ( $p > 0.1$ ). As one can see, both the flux and the strengthening are not affected by any of the drugs, while the variability is. However, differently from the amplitude, variability shows to be affected by drug B, being facilitatory and irreversible. Drug A also shows a irreversible and facilitatory effect on the variability but curiously with some delay. This may indicate that the time for drug application, while being properly

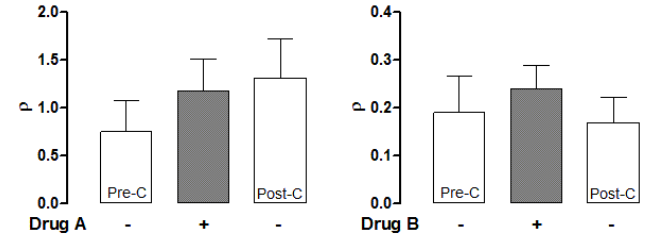


Figure 11: Correlations for drug A (top) and drug B (bottom) as shown in Eq. (7). For the period when applying drug B one observes  $\rho \sim 1/4$  meaning that the functional structure is random. Still, before and after the application of drug B, the correlation deviate from the purely random case. The same occurs for the experiments with drug A (see text).

used when evaluating its effect in total signal amplitude (Fig. 8) may be not long enough for other features of the tissue influencing the signal propagation, in this case the variability. Such increase of the variability could be a sign that the structure supporting some robustness of signal propagation is permanently modified by each drug. The same facilitatory and irreversible effect on the sensitivity seems to also occur, but only for drug A. It deserves to be noted that in a completely random model of link creation in each time step  $T$ , the variability would be peaked at a value of  $1/2$ . This is not supported by our data, which is a strong indicator that the reconstructed network do not have overwhelmingly random character.

For these new properties, we may summarize the analysis in this section by stating that while drug A mainly affects sensitivity  $\sigma/\langle w \rangle$ , drug B mainly affects variability  $\eta$ .

Comparing the variability  $\eta$  with the amplitude one concludes that, at least for these two different properties and for the correlation measure, the effects of the drugs are of different

nature. Therefore, one should approach such drug effects in a more extended way to analyze not only its overall influence in one single property, such as the total amplitude of the signals, but also in a set of properties that combined, characterize the functional structure of the network.

Finally, it is important to check whether the functional structure does not change randomly among the several experiments under the same conditions. Figure 11 shows the one-step correlation

$$\rho(T) = \frac{1}{L} \sum_{i \neq j} w_{ij}(T+1)w_{ij}(T) \quad (7)$$

for all three periods when testing drug A (left) and drug B (right). If we imagine a simple binomial model in which functional connections between cells  $i, j$  are randomly created in each step, i.e.  $w_{ij}(t) = \text{ran}(0, 1)$ , both correlations would be equal to  $1/4$ . Correlation values above  $1/4$  indicate the presence of actual correlations and memory about previous correlations in the system. When applying drug B correlations approximate the uncorrelated regime  $\rho = 1/4$ . For both pre and post periods however, correlation deviates significantly from  $\rho = 1/4$ , evidencing a functional structure underlying the sequence of signals. For drug A this deviation is even stronger and it is further strengthened when applying the drug in a irreversible way (check Tab. 1).

## 5. Conclusions

In this paper we introduce a procedure for extracting the functional connectivity network in living tissues subjected to external pulsed stimuli that propagate through it as a signal. Our method is based on the covariance matrix of the separated signals taken at different time-lags. By adding proper constraints of a minimum time-delay between pairs of cells and single-source stimulus to each cell we are able to filter out all redundant or artificial connections from the covariance matrix. We test our procedure with synthetic data. There, our procedure proves to be better suited for assessing the connectivity of living tissues of astrocytic samples used than other standard measures, namely the multivariate Granger causality algorithm. The better results of our procedure indicates that for the particular case of signal propagation networks with one single triggering source, standard methods may retrieve biased results.

The weight (strength) of each connection is computed directly from the covariance matrix and the minimum delay-time. Further, we showed how to obtain additional insight relative to the drug used for stimulating the source-cell only by analyzing the distribution of connectivity strengths (weights). From the first, second and third moment of the weight distribution we showed how to characterize respectively the signal flux and also the sensitivity and strengthening of the network underlying the signal propagation in the tissue. We also characterized the temporal stability of the network by its variability and a correlation measure, and found these measures to complement the information from the signal amplitude ratios.

Following what was introduced in the beginning of our paper, it is important to stress here that our method is not able to un-

cover the physical connectivity structure between cells and that it is also not aimed for studying particular features of the signal itself, such as the measurement noise[7]. While our method works for pulsed signals similar to the ones measured in the samples shown in Fig. A.12, as explained in Appendix A, and the variability already reflects implicitly the impact of measurement noise in the sample of signals, it would be interesting to extend this methodology further to situations where the measurement noise is significant.

To further validate our method, it would be interesting to test it with an empirical known drug whose effect in the propagating structure is known. To our knowledge, there is no such drug test, since they typically focus on the overall (sum) signal in the tissue and not in the features of its propagation throughout the tissue.

All in all, this study proposes a procedure complementary to the standard approach where only the overall amplitude is tested before, during and after the application of a given drug. Although it is not able to extract the physical interconnections between cells, our simple procedure provides a way for quantifying the functional connectivity in the tissue and to ascertain how it changes due to the application of drugs. The framework introduced here as well as the reported findings should now be used for a systematic pharmacological study. Other more sophisticated approaches, namely a spectral analysis[24] applied to these signal-propagation networks, could be useful. In this case larger tissues, having a larger number of astrocytes, are needed.

Finally, while the method introduced in this paper is based in constraints that give results for primary functional connections, some other interactions with a real physiological meaning could be further considered. Namely, there can be autocatalytic phenomena by self-stimulation, some signals could be reversible or multiple stimulation of one cell may occur in other situations. Forthcoming studies could further improve the ability for characterizing drug effects in living tissues by considering these more general effects, i.e. several time-lags, or local maxima of the matrix solution, so that a hierarchy of interactions could be determined.

## Acknowledgments

The authors thank Matthew Blow for his suggestions on the text. MP thanks *Ciência sem Fronteiras*, Brasil, Ref. MCT/CNPq/CsF/202611/2012-4. Financial support from *Fundação para a Ciência e a Tecnologia*, Portugal is acknowledged by FR (SFRH/BPD/65427/2009), SHV (SFRH/BPD/81627/2011), PGL (*Ciência 2007*) and also partial support under PEst-OE/FIS/UI0618/2011 and the binational program between FCT and DAAD, DRI/DAAD/1208/2013 by PGL and FR.

## Appendix A. Generation of synthetic data

In order to evaluate our method for reconstruction the connectivity network, we propose a simple signal propagation model with properties similar to those found in the experiment.



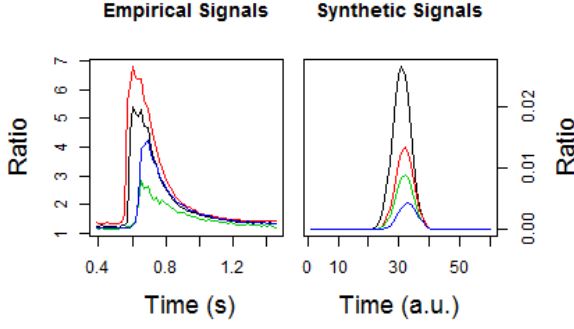


Figure A.12: Comparison between the empirical signals measured on astrocytic tissues and synthetic signals generated as described in Sec. Appendix A.

The model for signal propagation treats a set of nodes  $i$ ,  $i = 1, \dots, M$  with respective simulated signal time series  $\hat{X}_i(t)$  that are linked through connection with strength (weight)  $w_{ij}$ , either 0 or 1.

The signal propagation is governed by the following rules:

- i) The first node,  $i = 1$ , is driven by an external Gaussian signal  $\hat{X}_1(t) \propto \exp\left(-\frac{(t-t_0)^2}{2\sigma_0^2}\right)$ , where  $t_0$  is the starting time and  $\sigma_0$  is the standard deviation. Here we choose  $t_0 = 30$  and  $\sigma = 3$ .
- ii) Each node  $i \neq 1$  has only one incoming connection  $j$  ( $j \neq i$ ), i. e. only one nonvanishing  $w_{ji}$ .
- iii) There are no simple loops, i. e.  $w_{ii} = 0$ , for all  $i$ .
- iv) At each time step  $t$  the signal departing from cell  $i$  is distributed through its outgoing connections transporting the signal to its neighbors  $j$ . The distribution is implicitly defined as:

$$\hat{X}_i(t) = \alpha \sum_j w_{ij} \hat{X}_j(t + \tau_{ij}), \quad (\text{A.1})$$

with  $\alpha = 1/(1 + \sum_j w_{ij})$  and the delay  $\tau_{ij} = 1$  if  $w_{ij} = 1$  or  $\tau_{ij} = 0$  otherwise.

This means that the cells receive the incoming signal which is delayed by an amount in this case given by the strength of the incoming connections themselves. Such synthetic signals, while not having exactly the same shape as the empirical signals, do reproduce attenuation and stimulus delay in a similar way (see Fig. A.12).

## Appendix B. Granger causality

Granger causality procedures aim to test whether one time series is able to forecast another one. The main idea can easily be explained by considering, for simplicity, two time series  $X_1$  and  $X_2$ . One says that  $X_1$  Granger-cause  $X_2$  if the series of values of  $X_1$  provide information about future values of  $X_2$ . More precisely, we select a proper autoregression of  $X_2$  which has say  $m$  previous values

$$X_2^{(1)}(t) = a_0 + \sum_{i=1}^m a_i X_2(t-i) + \epsilon_t^{(1)}, \quad (\text{B.1})$$

and one computes the estimate errors  $\epsilon_t$ .

This autoregression is then compared with another one where the values of  $X_1$  are considered:

$$X_2^{(2)}(t) = a_0 + \sum_{i=1}^m a_i X_2(t-i) + \sum_{i=1}^m b_i X_1(t-i) + \epsilon_t^{(2)}. \quad (\text{B.2})$$

If the latter estimate error  $\epsilon_t^{(2)}$  is smaller then the former one  $\epsilon_t^{(1)}$ ,  $X_1$  is assumed to Granger-cause  $X_2$ .

In our paper we considered an improved multivariate version of Granger causality, where the  $M$  time-series are taken simultaneously and the error estimates of autoregressions are now for all pairs of variables and then compared as a matrix. Following the procedure outlined in [13], we fit to our vector of measured time series  $\mathbf{X}(t) = [X_1(t), X_2(t), \dots, X_M(t)]^T$  a MVAR (multivariate autoregressive) model as

$$\mathbf{X}(t) = \sum_{k=1}^p \mathbf{A}(k) \mathbf{X}(t-k) + \mathbf{E}(t) \quad (\text{B.3})$$

with a delay dependent coefficient matrix  $\mathbf{A}(k)$ , a given maximum delay  $p$ , and an error matrix  $\mathbf{E}$ , which are assumed to be Gaussian white noise sources. Transforming the quantities to the domain of frequencies  $f$ , one can compute the so-called transfer matrix  $\mathbf{H}(f)$  from the relation

$$\mathbf{A}^{-1}(f) \mathbf{E}(f) = \mathbf{H}(f) \mathbf{E}(f), \quad (\text{B.4})$$

from which one can compute the directed transfer function (DTF)  $\gamma$  as

$$\gamma_{ij}^2(f) = \frac{|H_{ij}(f)|^2}{\sum_{m=1}^M |H_{im}(f)|^2}. \quad (\text{B.5})$$

In a network of nodes  $i, j$ , the DTF is a measure of signal causality for the propagation of the signal from node  $j$  to node  $i$ . In our case, we use a single delay  $p = 1$ , effectively eliminating the frequency dependency of the DTF, which reduces to a matrix of connection strengths. It should be noted, however, that the multivariate Granger approach assumes stationarity of the underlying time series in order for the MVAR mechanism to be applicable. Stationarity does not hold in our case, as the measured signals are non-stochastic soliton-like peaks with a compact support. This is the fundamental reason for Granger causality to fail when applied to stimuli signals in living tissues.

## References

- [1] E.A. Newman, The Journal of Neuroscience **21**(7) 2215-2223 (2001).
- [2] P.G. Haydon, Nat. Rev. Neurosci. **2** 185-193 (2001).
- [3] O. Devinsky, A. Vezzani, S. Najjar, N.C. De Lanerolle, M.A. Rogawski, Trends in Neuroscience **36**, 174-184 (2013).
- [4] T. Hoefer, L. Venance, C. Giaume, J. Neurosci. **22** 4850-4859 (2002).
- [5] T.D. Hassinger, P.B. Guthrie, P.B. Atkinson, M.V.L. Bennet, S.B. Kater, Proc. Natl. Acad. Sci. **93** 13268-13273 (1996).
- [6] M.R. Bennett, L. Farnell, W.G. Gibson, Biophysical Journal **89** 2235-2250 (2005).
- [7] M. Perc, A.K. Green, C.J. Dixon, M. Marhl, Biophys. Chem. **132** 33-38 (2008).
- [8] M. Falcke, Advances in Physics **53** 255-440 (2004).
- [9] C. Giaume, L. Venance, Glia **24** 50-64 (1998)

- [10] A. Stozer, M. Gosak, J. Dolensek, M. Perc, M. Marhl, M.S. Rupnik and D. Korosak, PLOS Comp. Biol. **9** e1002923 (2013).
- [11] R. Diestel, *Graph Theory* (Springer-Verlag, Heidelberg, 2005).
- [12] C.W.J. Granger, *Econometrica* **37**, 424-438 (1969).
- [13] K.J. Blinowska, R. Kuś, M. Kamiński, *Physical Review E* **70**, 050902(R) (2004).
- [14] M. Dhamala, G. Rangarajan, M. Ding, *Physical Review Letters* **100** 018701 (2008).
- [15] C.W.J. Granger and M. Hatanaka, *Spectral analysis of economic time series* (Princeton Univ. Press, Princeton, 1964).
- [16] C.W.J. Granger and P. Newbold *Forecasting economic time series* (Academic Press, New York, 1977).
- [17] R. Sedgewick, *Algorithms* (Addison-Wesley, Reading, 1983).
- [18] A.H. Cornell-Bell, S.M. Finkbeiner, M.S. Cooper and S.J. Smith, *Science* **247** 470-473 (1990).
- [19] M. Kang and H.G. Othmer, *Chaos* **19** 037116 (2009).
- [20] S.H. Vaz, T.N.Jørgensen, S.Cristóvão-Ferreira, S.Duflot, J.A.Ribeiro, U.Gether and A.M.Sebastião, *J. Biol. Chem.* **286** 40464-40476 (2011).
- [21] K.D.McCarthy and J.de Vellis, *J. Cell Biol.* **85** 890-902 (1980).
- [22] C.R.Rose, R.Blum, B.Pichler, A.Lepier, K.W.Kafitz and A.Konnerth, *Nature* **426** 74-78 (2003).
- [23] S. Cristóvão-Ferreira, G. Navarro, M. Brugarolas, K. Pérez-Capote, S.H. Vaz, G. Fattorini, F. Conti, C. Lluis, J.A. Ribeiro, P.J. McCormick, V. Casadó, R. Franco, A.M. Sebastião, *Purinergic Signalling* **9** 433-449 (2013).
- [24] A.E. Brouwer, W.H. Haemers *Spectra of graphs* (Springer, New York, 2011).